Monthly Notices
of the
ROYAL ASTRONOMICAL SOCIETY

Mon. Not. R. Astron. Soc. **413,** 386–400 (2011) doi:10.1111/j.1365-2966.2010.18143.x

The REFLEX II galaxy cluster survey: power spectrum analysis

A. Balaguera-Antolínez,[1⋆] Ariel G. Sánchez,[1] H. Böhringer,[1] C. Collins,[2] L. Guzzo[3] and S. Phleps[1]

[1]*Max-Planck-Institut für extraterrestrische Physik, D-85748 Garching, Germany*
[2]*Liverpool John Moores University, 2 Rodney Street, Liverpool L3 5UX*
[3]*INAF, Osservatorio Astronomico di Brera, Milano, Italy*

Accepted 2010 December 2. Received 2010 November 12; in original form 2010 August 23

ABSTRACT

We present the power spectrum of galaxy clusters measured from the new *ROSAT*-ESO Flux-Limited X-Ray (REFLEX II) galaxy cluster catalogue. This new sample extends the flux limit of the original REFLEX catalogue to $1.8 \times 10^{-12}\,\mathrm{erg\,s^{-1}\,cm^{-2}}$, yielding a total of 911 clusters with $\geq$94 per cent completeness in redshift follow-up. The analysis of the data is improved by creating a set of 100 REFLEX II-catalogue-like mock galaxy cluster catalogues built from a suite of large-volume Λ cold dark matter (ΛCDM) N-body simulations (L-BASICC II). The measured power spectrum is in agreement with the predictions from a ΛCDM cosmological model. The measurements show the expected increase in the amplitude of the power spectrum with increasing X-ray luminosity. On large scales, we show that the shape of the measured power spectrum is compatible with a scale-independent bias and provide a model for the amplitude that allows us to connect our measurements with a cosmological model. By implementing a luminosity-dependent power-spectrum estimator, we observe that the power spectrum measured from the REFLEX II sample is weakly affected by flux-selection effects. The shape of the measured power spectrum is compatible with a featureless power spectrum on scales $k > 0.01\,h\,\mathrm{Mpc}^{-1}$ and hence no statistically significant signal of baryonic acoustic oscillations can be detected. We show that the measured REFLEX II power spectrum displays signatures of non-linear evolution.

Key words: galaxies: clusters: general – cosmology: theory – large-scale structure of Universe – X-rays: galaxies: clusters.

1 INTRODUCTION

Within the last decade, three foundational observational probes have been well recognized as opening-up observational windows to reveal some of the most valuable secrets of the Universe. These are the temperature fluctuations of the cosmic microwave background (CMB) radiation, recently measured with high precision by the *Wilkinson Microwave Anisotropy Probe* satellite (Spergel et al. 2007; Komatsu et al. 2010), the *Hubble* diagram inferred from the Type Ia supernova observations (e.g. Perlmutter et al. 1999; Riess, Strolger & Tony 2004) and the measurement of the large-scale structure (LSS) of the Universe as traced by the spatial distribution of galaxies (Percival et al. 2002; Sánchez et al. 2006; Tegmark et al. 2006; Percival et al. 2007, 2010; Reid et al. 2010).

With the completion of large redshift surveys, such as the Two-degree Field Galaxy Redshift Survey (2dFGRS)[1] and the Sloan Digital Sky Survey (SDSS),[2] it has been possible to push the level of accuracy of LSS studies. The recent detection of the baryon acoustic oscillations (BAOs, e.g. Cole et al. 2005; Eisenstein et al. 2005; Gaztañaga, Cabré & Hui 2008; Sánchez et al. 2009; Percival et al. 2010) in redshift surveys has been key to this progress. Over the last few years, these observations have established the concordance cosmological model, based on a flat space–time in a current phase of accelerated expansion due to the presence of a dominating dark energy component, whose equation of state is compatible with Einstein's cosmological constant Λ. This is the so-called Λ cold dark matter (ΛCDM) cosmological model.

Galaxy cluster samples also provide valuable information to obtain constraints on cosmological parameters. Galaxy clusters are the largest bounded structures in the Universe. They are associated with the highest peaks in the matter density field and are recognized as biased tracers of the underlying matter distribution (e.g. Bardeen et al. 1986). Their deep potential wells make them the largest

⋆E-mail: abalan@mpe.mpg.de
[1]http://msowww.anu.edu.au/2dFGRS/
[2]http://www.sdss.org/

astrophysical laboratories in the Universe, where the combination of gravitation and baryonic physics has been intensively studied through the analysis of cluster properties, such as scaling relations (e.g. Reiprich & Böhringer 1999; Pratt et al. 2009; Mantz et al. 2010), density profiles (e.g. Makino, Sasaki & Suto 1998), pressure profiles (e.g. Arnaud et al. 2010), baryon fractions (e.g. Giodini et al. 2009), etc. The abundances of galaxy clusters determined by their luminosity function (e.g. Böhringer et al. 2002) can also be used to constrain parameters like the matter content in the universe, $\Omega_{\rm m}$, and the amplitude of the density fluctuations characterized by σ_8, the rms linear perturbation theory variance in spheres of radius $8\,{\rm Mpc}\,h^{-1}$ (e.g. Schuecker et al. 2003). The spatial distribution of galaxy clusters, characterized by its power spectrum (or correlation function), provides useful information about the cosmological model of the Universe. The shape of this measurement is particularly sensitive to the parameter combination $\Omega_{\rm m}\,h$, which complements the constraints on these parameters obtained from the analysis of fluctuations in the CMB radiation. Furthermore, the amplitude of the galaxy cluster power spectrum also contains important information that can be related to theoretical models in a more direct way than for measurements based on galaxy samples (e.g. Moscardini et al. 2000).

In the past few years, the *ROSAT*-ESO Flux-Limited X-Ray (REFLEX) catalogue (Böhringer et al. 2001) has been used to measure fundamental cosmological quantities. The REFLEX catalogue is based on *ROSAT* All Sky Survey (RASS) observations (Truemper 1993), complemented with follow-up observations as described by Guzzo et al. (2009), yielding spectroscopic redshifts for 447 clusters with flux limit of $3 \times 10^{-12}\,{\rm erg\,s^{-1}\,cm^{-2}}$ (in the *ROSAT* energy band 0.1–2.4 keV). The REFLEX catalogue was, to date, the largest statistically complete X-ray-detected cluster sample. The clustering properties of this survey were analysed by means of the power spectrum (Schuecker et al. 2001), the cluster correlation function (Collins et al. 2000), cluster-galaxy cross-correlation functions (Sánchez et al. 2005) and Minkowski functionals (Kerscher et al. 2001). Subsamples of the REFLEX catalogue complemented by detailed follow-up observations have been used to constrain cluster scaling relations (e.g. Reiprich & Böhringer 1999; Stanek et al. 2006; Pratt et al. 2009; Mantz et al. 2010).

In this paper, we present the analysis of the power spectrum of the new REFLEX II catalogue. The REFLEX II catalogue is an extension of the REFLEX catalogue to a lower limiting flux ($1.8 \times 10^{-12}\,{\rm erg\,s^{-1}\,cm^{-2}}$) allowing the inclusion of 464 new clusters over the original sample and yielding a total of 911 clusters with spectroscopic redshifts for ∼95 per cent of the sample.

In addition to the enlarged sample size of the REFLEX II catalogue, several improvements were made to the data reduction: (i) we use the RASS product RASS III which gives a few per cent more sky exposure in formerly underexposed areas due to improved attitude solutions, consequently recovering a few more clusters at higher flux; (ii) for the count rate to flux conversion, an estimated temperature has to be applied, which is now obtained with up-to-date scaling relations based on the REXCESS (Böhringer et al. 2007) with the *L*–*T* relation described in Pratt et al. (2009); and (iii) the total flux and X-ray luminosity is now estimated inside the radii of r_{500} and r_{200} (based on relations described in Pratt et al. 2009; Arnaud, Pointecouteau & Pratt 2005). These calculations now involve less extrapolation than the estimates for the previously used fiducial radius.

Besides the advantages provided by a larger cluster sample, the power spectrum analysis presented here represents an improvement over that of Schuecker et al. (2001) in a number of ways. In particular, our analysis is complemented with a set of *N*-body simulations, the L-BASICC II (Angulo et al. 2008; Sánchez, Baugh & Angulo 2008a), from which we constructed a suite of 100 REFLEX II mock catalogues. These catalogues were calibrated to reproduce the measured REFLEX II X-ray luminosity function. Selection criteria of the REFLEX II sample were applied in their construction, yielding a large suite of mocks that can be used to analyse the statistical methods applied to the data. The details of the construction of these mock catalogues will be described in a forthcoming paper (Sánchez et. al., in preparation).

Our ensemble of mock catalogues allowed us to show that it is possible to construct an accurate model of the shape and amplitude of the REFLEX II power spectrum. This model includes the effects of the non-linear evolution of density fluctuations, redshift-space distortions and halo bias, which introduce deviations in the clustering signal with respect to the simple predictions of linear perturbation theory. This will allow us to use the full information contained in the REFLEX II power spectrum to obtain constraints on cosmological parameters.

This paper is organized as follows. In Section 2, we describe the REFLEX II sample and the survey selection function, followed by a brief description of the construction of the mock catalogues in Section 2.3. In Section 3, we describe the power-spectrum estimator and show the measurements of the REFLEX II window function and the covariance matrix. In Section 4.1, we model the amplitude of the power spectrum measured from the mock catalogues. In Section 4.2, we explore the sensitivity of the REFLEX II sample to distortions induced by flux-selection effects. In Section 4.3, we model the shape of the power spectrum. The model of the shape and the amplitude is applied to the REFLEX II sample in Section 5. We end with our conclusions in Section 6.

Our fiducial cosmological model consists of a flat ΛCDM Universe with a matter energy density parameter of $\Omega_{\rm m} = 0.25$, a dark energy equation of state $w = -1$, a dimensionless Hubble parameter $h = 0.7$[3] and a spectral index of primordial scalar fluctuations $n_{\rm s} = 1$. Throughout this paper, we refer to the X-ray luminosity in the *ROSAT* hard energy band 0.1–2.4 keV and, whenever it is not explicitly written, its units are given in $10^{44}\,{\rm erg\,s^{-1}}\,h^{-2}$.

2 THE REFLEX II GALAXY CLUSTER CATALOGUE

2.1 Catalogue construction

Fig. 1 shows the angular positions of the 911 galaxy clusters of the REFLEX II sample. The catalogue covers $13\,924\,{\rm deg^2}$ (4.24 sr) in the Southern hemisphere ($\delta < 2.^{\circ}5$) where the Milky Way and the Magellanic Clouds have been excised to avoid contamination due to stars and regions with high-X-ray-absorbing neutral hydrogen column density and high extinction in the optical band. The limiting flux of the REFLEX II sample is $1.8 \times 10^{-12}\,{\rm erg\,s^{-1}\,cm^{-2}}$ and includes 464 new clusters in addition to the original REFLEX sample, which had 447 clusters to a limiting flux of $3 \times 10^{-12}\,{\rm erg\,s^{-1}\,cm^{-2}}$. The detection technique is the same as that developed for the REFLEX sample (Böhringer et al. 2001; Guzzo et al. 2009), with spectroscopic redshifts for 860 clusters and spanning luminosities in the range $4.9 \times 10^{40} \leq L_{\rm X}/({\rm erg\,s^{-1}}\,h^{-2}) \leq 1.96 \times 10^{45}$. The missing ≈6 per cent of the redshifts will be obtained in observations made at La Silla in fall of 2010 and spring 2011. The angular distribution of X-ray clusters without redshift in the REFLEX II sample is also

[3]The Hubble constant H_0 in units of $100\,{\rm km\,s^{-1}\,Mpc^{-1}}$.

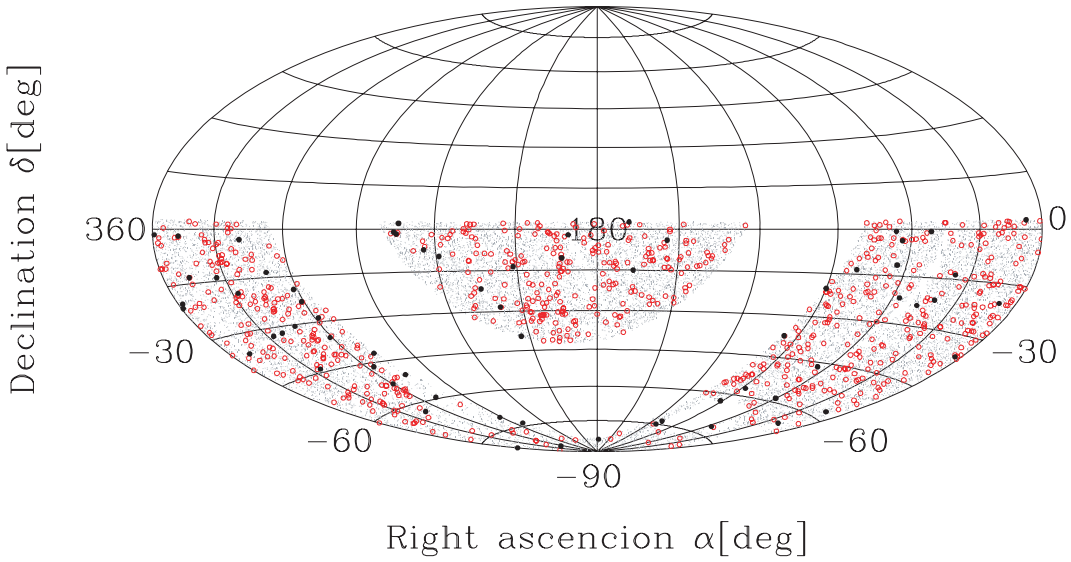

Figure 1. Distribution of REFLEX II clusters in equatorial coordinates. Open circles represent the position of the REFLEX II clusters. Filled circles represent the REFLEX II clusters without redshift. The points represent 5 per cent of the random catalogue constructed with the REFLEX II selection function. The empty regions in the Southern hemisphere correspond to the cut in galactic coordinates $|b_{\rm II}| < 20^\circ$ of the Milky Way (band) and the Magellanic Clouds.

shown in Fig. 1 (filled circles), displaying no particular pattern on the sky. We estimate that our results will not change substantially due to this incompleteness.

While a more detailed description of the sample construction and the derivation of the cluster parameters will be given in a forthcoming paper (Böhringer et al., in preparation), we provide here a brief description of these measurements and calculations. Source counts for the galaxy clusters in the RASS have been determined in the 0.5–2 keV energy band by means of the growth curve analysis method described in Böhringer et al. (2000). The growth curve method is tailored to maximize the aperture in which the source counts are determined. The count rate (obtained by reference to the exposure maps of the RASS) is then converted to a nominal flux, $F_{\rm n}$, by means of XSPEC (Arnaud 1996) assuming a MEKAL plasma model for a cluster temperature of 5 keV, a redshift of $z = 0$, a metallicity of 0.3 solar and a value for the hydrogen column density taken from the measurements of Dickey & Lockman (1993). The flux limit is imposed on the cluster sample using this value of $F_{\rm n}$. For clusters whose redshifts are known, an improved flux value, $F_{\rm X}$, is determined by recalculating the count rate to flux conversion for a temperature estimated via the X-ray luminosity–temperature relation as given by Pratt et al. (2009) and by including the proper band corrections (analogous to the optical K-correction) for the actual cluster redshift. The measured flux is converted to an estimated flux within an aperture radius of r_{500} (the radius in which the mean matter density of the cluster is 500 times the critical density of the Universe) by means of relations given in Pratt et al. (2009). The flux extrapolation (and in some cases interpolation) is achieved by assuming a cluster surface brightness following a β-model (Cavaliere & Fusco-Formiano 1976) with $\beta = 2/3$ and core radius $r_{\rm c} = (1/7)r_{500}$. The cluster rest-frame X-ray luminosity is calculated by means of the luminosity distance from $F_{\rm X}$, taking the proper band corrections for the redshift into account.

For the determination of the sky-position-dependent selection function, the minimum luminosity as a function of redshift and the position on the sky $L_{\rm X}^{\rm lim}$ (α, δ, z) is calculated assuming the nominal flux limit and taking into account that for 5.4 per cent of the sky the exposure is too short (<100 s, mostly due to instrument shut-down during passages of the radiation belts in South Atlantic Anomaly) to reach the nominal flux limit. The values of $L_{\rm X}^{\rm lim}$ (α, δ, z) are then derived by accounting for the proper $F_{\rm X}$ for given redshift and by performing an iterative backward engineering of the above-described process. The surveyed area defining the REFLEX II sample has been divided into $N_{\rm pix} = 13\,902$ pixels with an area $\approx$1 deg^2. For each pixel centred on equatorial coordinates (α_i, δ_i), the limiting luminosity $L_{\rm X}^{\rm lim}$ (α_i, δ_i, z) was tabulated in the range $0 \leq z \leq 0.8$. Given the minimum count rate of 20 counts and the geometrical boundaries of the survey (see table 1 of Böhringer et al. 2001), we end up with a total of 787 galaxy clusters.

2.2 The REFLEX II selection function

We measured the REFLEX II X-ray luminosity function using the $V_{\rm max}$ estimator. We fitted the measurements by means of what we call an *extended Schechter function*,

$$\Phi(L_{\rm X}){\rm d}L_{\rm X} = n_0 \left(\frac{L_{\rm X}}{L_\star}\right)^{\alpha} {\rm e}_q(x)\frac{{\rm d}L_{\rm X}}{L_\star}, \tag{1}$$

where e $_q(x)$ denotes the so-called q-exponential function (e.g. Tsallis 2009) defined as

$${\rm e}_q(x) \equiv \begin{cases} {\rm e}^x & q = 1, \\ (1 + x(1-q))^{1/(1-q)} & q \neq 1. \end{cases} \tag{2}$$

This parametrization provides a better description of the high-luminosity tail of the X-ray luminosity function (Sánchez et al., in preparation). We implemented a Markov chain Monte Carlo (MCMC) technique to determine the best-fitting parameters (n_0, α, $L_\star$, q) given by

$$\begin{aligned} n_0 &= \left(4.081^{+0.012}_{-0.010}\right) \times 10^{-6}\ \left({\rm Mpc}\,h^{-1}\right)^{-3}, \\ \alpha &= -1.536^{+0.006}_{-0.013}, \\ L_\star &= \left(0.6283^{+0.031}_{-0.028}\right) \times 10^{44}\,{\rm erg\,s^{-1}}\,h^{-2}\ \text{and} \\ q &= 1.313^{+0.010}_{-0.013}. \end{aligned} \tag{3}$$

In order to explore the behaviour of the clustering strength as a function of X-ray luminosity, we split the REFLEX II sample into

Table 1. Minimum X-ray luminosities $L_i^{\rm min}$ ($i = 1, \ldots, 6$) used to define subsamples of the REFLEX II catalogue, with a maximum redshift $z_{\rm max} = 0.22$. N_i denotes the number of clusters in each subsample and $\bar{z}_i$ is the corresponding mean redshift. $N_{\rm VLS}$ is the number of REFLEX II clusters and $\bar{n}_{\rm VLS}$ is the mean density in each volume-limited sample in units of 10^{-6} (Mpc $h^{-1})^{-3}$. X-ray luminosity is in units of 10^{44} erg s^{-1} h^{-2} in the energy band 0.1–2.4 keV.

Sample i	$L_i^{\rm min}$	N_i	$\bar{z}_i$	$N_{\rm VLS}$	$\bar{n}_{\rm VLS}$
1	0.015	661	0.070	32	4.318
2	0.049	625	0.080	90	1.856
3	0.154	512	0.099	150	0.6562
4	0.245	441	0.112	159	0.3905
5	0.490	306	0.136	154	0.1535
6	0.588	260	0.143	157	0.1155

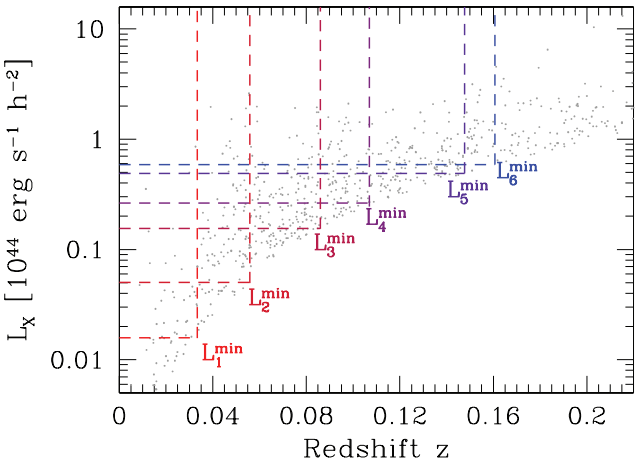

Figure 2. Luminosity–redshift diagram for the REFLEX II sample (points). Dashed lines schematically represent the volume-limited samples defined by the limiting luminosities of Table 1.

six subsamples characterized by a minimum luminosity $L_i^{\rm min}$. These are listed in Table 1, together with their corresponding number of clusters N_i and mean redshift $\bar{z}_i$. For a given luminosity cut $L_i^{\rm min}$, the expected number density at a position $\boldsymbol{r}$, characterized by angular coordinates (α, δ) and redshift z, is obtained via integration of the X-ray luminosity function as

$$\bar{n}\left(\boldsymbol{r}; L_i^{\rm min}\right) = \int_{\hat{L}(\boldsymbol{r})}^{\infty} \Phi(L_{\rm X}) {\rm d}L_{\rm X}, \quad (4)$$

where the lower integration limit $\hat{L}(\boldsymbol{r})$ is given by the REFLEX II sensitivity map as

$$\hat{L}(\boldsymbol{r}) \equiv {\rm Max}\left(L_i^{\rm min}, L_{\rm X}^{\rm lim}(\alpha, \delta, z)\right). \quad (5)$$

We also constructed six volume-limited samples (VLSs) using the same minimum luminosities. These VLSs are schematically represented in Fig. 2. Table 1 also lists the number of clusters, the mean redshift and the cluster number density for these subsamples.

Finally, we created a random catalogue of $N_{\rm r} = 2 \times 10^6$ objects with luminosities greater than $L_{\rm X} = 1.4 \times 10^{43}$ erg s^{-1} h^{-2}. In Fig. 1, we show the angular positions of a subset of the random sample. Note the variations in the angular distribution of the random catalogue, which follow the fluctuations in the sensitivity map of the REFLEX II survey.

2.3 The mock catalogues

In this section, we give a short outline of the construction of a suite of REFLEX II mock catalogues. A more detailed description and analysis will be given in a forthcoming paper (Sánchez et al., in preparation).

We used the $z = 0$ output of the 50 realizations from the L-BASICC II N-body simulations (Angulo et al. 2008; Sánchez et al. 2008a) to generate a suite of REFLEX II mock catalogues. The cosmological model adopted in the simulations consists of a flat ΛCDM universe with a matter energy density parameter $\Omega_{\rm m} = 0.237$, a baryon energy density parameter of $\Omega_{\rm b} = 0.046$, a dimensionless Hubble parameter $h = 0.73$, a dark energy equation of state $w = -1$ and an initial matter power spectrum characterized by a scalar spectral index $n_{\rm s} = 0.954$ and normalized to $\sigma_8 = 0.77$, which is in close agreement with the latest constraints on cosmological parameters from CMB and LSS measurements (e.g. Sánchez et al. 2006; Spergel et al. 2007; Sánchez et al. 2009; Komatsu et al. 2010). The low value of σ_8 is particularly important in order to obtain cluster number counts in accordance with observations.

Each of the L-BASICC II simulations follows the dark matter distribution using 448^3 particles over a comoving box of side 1.34 Gpc h^{-1}. We used halo catalogues identified via a friend-of-friend (FoF) algorithm with a linking length of $b = 0.2$. The resulting halo-mass resolution is $M = 1.75 \times 10^{13}\,{\rm M}_\odot\, h^{-1}$.

We assigned luminosities to the dark matter haloes in the simulations using a mass–luminosity M–$L_{\rm X}$ relation with an intrinsic scatter $\sigma_{\ln L} = 0.26$. This value was measured by Stanek et al. (2006) under the assumption of a flat cosmological model with $\Omega_{\rm m} = 0.24$, close to our fiducial cosmology. Flux errors are included in the luminosity assignment by assuming a fixed error in $L_{\rm X}$ of $\delta L_{\rm X}/L_{\rm X} =$ 20 per cent, which characterizes the flux errors in the REFLEX II sample fairly well. For the mean M–$L_{\rm X}$ relation, we assumed a power law with a mass-dependent slope. Setting

$$\ell = \log_{10}\left(\frac{\bar{L}_{\rm X}}{10^{44}\,{\rm erg\,s^{-1}}\,h^{-2}}\right), \quad m = \log_{10}\left(\frac{M}{10^{14}\,{\rm M}_\odot\,h^{-1}}\right), \quad (6)$$

our mass–luminosity relation reads

$$\ell = a + bm + cm^2. \quad (7)$$

Using a MCMC technique, we calibrated the set of coefficients (a, b, c) such that the resulting luminosity distribution of the illuminated dark matter haloes matches the measured X-ray luminosity function from the REFLEX II sample. The best-fitting values are $a = -1.3164, b = 1.8769$ and $c = -0.2955$. Changes below 1 per cent in these parameters are observed when the flux error is reduced to 10 per cent, although this value underestimates the observed flux errors of the REFLEX II sample. The goodness of this self-calibration is confirmed by comparing the REFLEX II luminosity function and the mean luminosity function determined from the mock catalogues, obtaining differences of $\lesssim$3 per cent. Interestingly, this calibration of the M–$L_{\rm X}$ relation shows a deviation from the power-law behaviour at low luminosities. This is in agreement with recent observations and N-body hydrosimulations (Puchwein, Sijacki & Springel 2008; Stanek et al. 2010). Nevertheless, we do not attempt to extract conclusions on the underlying mass–luminosity relation for a number of reasons. First, the FoF halo-finder algorithms overestimate the halo mass due to systematics introduced by the finite number of particles used to define a dark matter halo. Warren et al. (2006) showed a way to correct for these systematics, which only depends on the FoF mass. For the lowest luminosity cut shown in Table 1, the distribution of minimum halo masses selected by equation (7) in the mocks peaks at

$M \approx 5 \times 10^{13}\,\mathrm{M}_{\odot}\,h^{-1}$, which, following the correction of Warren et al. (2006), corresponds to an offset of ∼40 per cent with respect to unbiased mass estimations. Nevertheless, we do not attempt to correct the L-BASICC II FoF masses, for any correction would lead to a new set of parameters (a, b, c) which will still reproduce, by construction, the observed X-ray luminosity function. Secondly, there is not a clear one-to-one relation between FoF masses and the spherical overdensity masses (e.g. Lukic et al. 2010), which are usually implemented in the calibration of cluster scaling relations (e.g. Pratt et al. 2009).

We next transformed the coordinates of the haloes to redshift space using $r \rightarrow r + \boldsymbol{v}\cdot\hat{\boldsymbol{r}}/H_0$, where $\boldsymbol{v}$ is the peculiar velocity of the centre of mass of the haloes. We neglected spectroscopic redshift errors for being of the order of $\sigma \sim 10^{-3}$ (Guzzo et al. 2009). Finally, we observed the illuminated haloes through the REFLEX II mask and obtained a set of mock catalogues with the abundance and geometry in agreement with those of the REFLEX II sample.

We constructed two sets of mocks. One set consists of 50 mocks covering the full volume of the REFLEX II sample (out to $z \approx 0.5$). For the second set, we noted that the effective volume of the REFLEX II sample reaches a maximum at redshift $z \approx 0.2$ (see Section 3.2). Therefore, including clusters with higher redshift will not help to improve the signal-to-noise ratio of the measurements. For this reason, we set a maximum redshift of $z = 0.22$ which allowed us to construct 100 independent mock catalogues out of the 50 L-BASICC II realizations. Unless otherwise stated, we use the set of 100 mocks to carry out our statistical analysis. The set of 50 mocks were used for consistency checks.

In the analysis of the REFLEX power spectrum, Schuecker et al. (2001) constructed 10 mock catalogues by assigning X-ray luminosities to the dark matter haloes in a small set of N-body simulations using the M–L_{X} relation of Reiprich & Böhringer (1999). No intrinsic scatter around the mean M–L_{X} relation, flux errors or missing flux corrections were introduced in the mocks. Note that this difference with respect to our analysis will result in a different prediction of the amplitude of the power spectrum for a given luminosity cut. In Section 5.2, we address the modelling of the amplitude of the power spectrum, taking these details into account.

3 METHODS

3.1 The measurement of $P(k)$

We have measured the power spectrum of the REFLEX II sample containing clusters with luminosities $L_{\mathrm{X}} \geq L_1^{\mathrm{min}}$, which represents 760 objects in the redshift interval covered by the REFLEX II survey. We implemented the standard minimum variance weighting power-spectrum estimator of Feldman, Kaiser & Peacock 1994 (hereinafter FKP), which defines a weighted density fluctuation

$$F(\boldsymbol{r}) = w(\boldsymbol{r})\,[n_{\mathrm{c}}(\boldsymbol{r}) - \alpha n_{\mathrm{r}}(\boldsymbol{r})]\,, \tag{8}$$

where $n_{\mathrm{c}}(\boldsymbol{r})$ ($n_{\mathrm{r}}(\boldsymbol{r})$) is the number density of clusters in the real (random) catalogue for a given luminosity cut (where we dropped the L^{min} dependence to avoid clutter). The parameter α given by

$$\alpha = \frac{\int w(\boldsymbol{r}) n_{\mathrm{c}}(\boldsymbol{r})\,\mathrm{d}^3 r}{\int w(\boldsymbol{r}) n_{\mathrm{r}}(\boldsymbol{r})\,\mathrm{d}^3 r}, \tag{9}$$

forces the fluctuation to have zero mean, $\int F(\boldsymbol{r})\,\mathrm{d}^3 r = 0$. The optimal normalized weights $w(\boldsymbol{r})$ are given by FKP:

$$w(\boldsymbol{r}) = \left[\frac{1}{1+\bar{n}(\boldsymbol{r})P_{\mathrm{est}}}\right]\left[\int \frac{\bar{n}(\boldsymbol{r})}{1+\bar{n}(\boldsymbol{r})P_{\mathrm{est}}}\,\mathrm{d}^3 r\right]^{-1}, \tag{10}$$

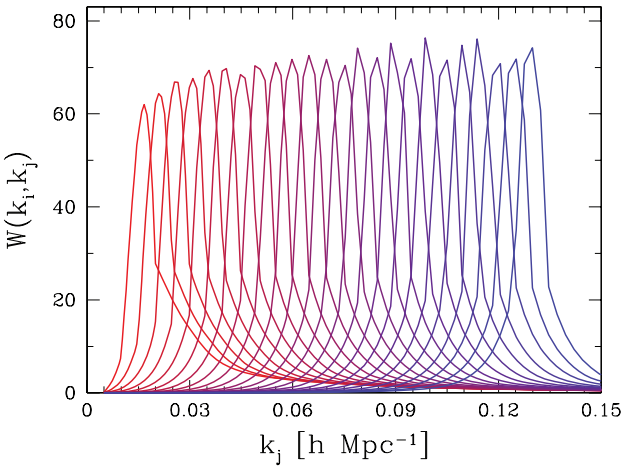

Figure 3. Example of the REFLEX II shell averaged window (matrix) function W_{ij} for different modes k_i determined for the subsample with limiting luminosity L_2^{min}. Each curve is normalized to $\int \mathrm{d}k_j\, W(k_i, k_j) = 1$.

where P_{est} is an estimate of the amplitude of the power spectrum expected to be measured, for which we have chosen $P_{\mathrm{est}} = 2 \times 10^4\ (\mathrm{Mpc}\,h^{-1})^3$. We used the FFTW algorithm (Frigo & Johnson 2005) embedding the REFLEX II volume in a cube divided into $N_{\mathrm{grid}} = 512^3$ cells and implemented a triangular-shaped cloud mass assignment (Hockney & Eastwood 1988) correcting afterwards for aliasing effects. The length of the sides of the cube is determined by $L_{\mathrm{box}} = 2r(z_{\mathrm{max}})$, with $z_{\mathrm{max}} = 0.22$ which corresponds to a box size of $1.25\,\mathrm{Gpc}\,h^{-1}$ for our fiducial cosmology. The fundamental mode is $\Delta k = 2\pi/L_{\mathrm{box}} = 0.0049\,h\,\mathrm{Mpc}^{-1}$. The Nyquist frequency for this box is $k_{\mathrm{Nyq}} = 1.27\,h\,\mathrm{Mpc}^{-1}$ and we can ignore aliasing effects on wavenumbers smaller than $k \approx 0.7\,h\,\mathrm{Mpc}^{-1}$. We subtract the shot noise and average in spherical shells to obtain the bin-averaged power spectrum $\hat{P}(k)$. This measurement is the convolution of the underlying cluster power spectrum with $|W(\boldsymbol{k})|^2$, the square of the Fourier transform of the REFLEX II window function given by

$$W(\boldsymbol{k}) = \int \bar{n}(\boldsymbol{r})\, w(\boldsymbol{r}) \mathrm{e}^{-\mathrm{i}\boldsymbol{k}\cdot\boldsymbol{r}}\,\mathrm{d}^3 r. \tag{11}$$

We follow the procedure of Cole et al. (2005) to construct the window function in matrix form W_{ij}, by using a Gauss–Legendre integration scheme (Press et al. 2002). The measured power spectrum can be written as a matrix multiplication

$$\hat{P}(k_i) = \sum_j W_{ij}\, P(k_j) - W_{i0}, \tag{12}$$

where $P(k_j)$ is the underlying power spectrum and the term W_{i0} accounts for the integral constraint (Percival et al. 2007; Reid et al. 2010). As an example, Fig. 3 shows some elements of the window matrix of the sample defined by the minimum luminosity L_2^{min} (panel a) and the volume-limited sample defined by the same luminosity cut (panel b). As expected, large-scale modes receive contributions from intermediate to even small ($k \geq 0.3\,h\,\mathrm{Mpc}^{-1}$) scales.

We used the window matrix to asses the possibility of detecting the signal of the BAO in the measured REFLEX II power spectrum. The signature of BAOs in the dark matter halo distribution of the L-BASICC II simulations has been analysed both in the spatial two-point correlation function (Sánchez et al. 2008a) and in the power spectrum (Angulo et al. 2008). We used the fitting formulae of Eisenstein & Hu (1998) to compute the matter power spectrum for the cosmological model of the L-BASICC II simulations,

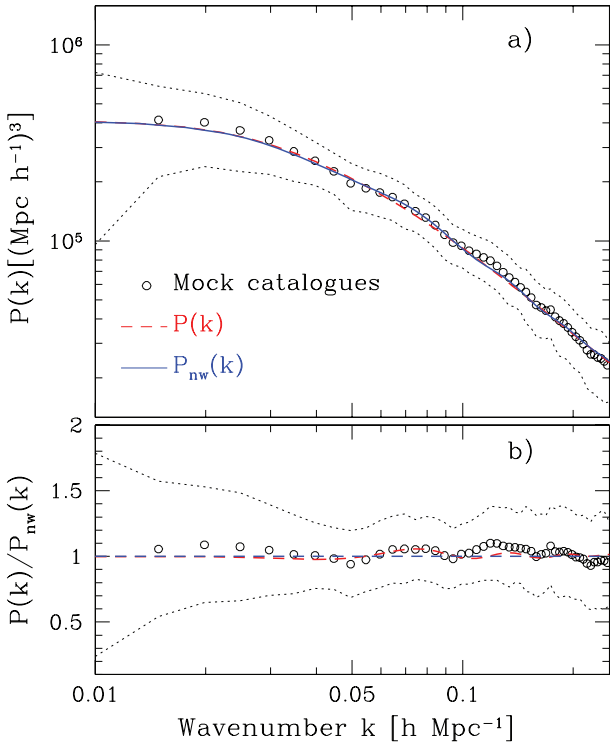

Figure 4. Panel (a): mean power spectrum from the mock catalogues (open points), with its corresponding standard deviation (dotted lines), for the subsample characterized with the limiting luminosity $L_2^{\rm min}$. The solid line $P_{\rm nw}(k)$ represents a non-linear matter power spectrum $P(k)$ without BAOs and convolved with the REFLEX II window function. The dashed line represents the same theoretical prediction with BAOs, also convolved with the window function. Panel (b): ratio of the mean mock power spectrum (open points) and the power spectrum $P(k)$ to the power spectrum $P_{\rm nw}(k)$. Dotted lines denote the 1σ standard deviation.

including a non-linear correction computed with HALOFIT (Smith et al. 2003). We also computed a model with the same broad-band shape but without any baryonic oscillations, $P_{\rm nw}(k)$, provided as well by Eisenstein & Hu (1998). Fig. 4 (panel a) shows the comparison of these theoretical models (solid and dashed lines), convolved with the REFLEX II window function, with the mean power spectrum from the mock catalogues (open circles). It can be seen that the difference between these two models is much smaller than the standard deviation in $P(k)$ that corresponds to the REFLEX II volume, which can be determined from the ensemble of mock catalogues (dotted lines, see Section 3.2). This can be more clearly seen in panel (b) of the same figure, which shows the ratio of these power spectra to $P_{\rm nw}(k)$. The convolution with the window function damps the acoustic oscillations in the power spectrum to a level where they cannot be distinguished from a model without BAOs. Furthermore, we computed χ^2 of these two models (analytically marginalizing over the amplitude as described in Lewis & Bridle 2002) and found a difference of less than $\sim$3 per cent between them. We thus conclude that, due to the survey volume, no statistically significant signal of BAOs can be detected in the REFLEX II power spectrum.

A detection of BAO signatures in a galaxy cluster sample was claimed by Miller, Nichol & Batuski (2001) based on the measurements of the power spectrum of the Abell/ACO cluster survey (Miller et al. 2001). This claim was based on different statistical methods from the ones applied in this work and no mock catalogues were used to assess the statistical significance of the detection. Our cluster sample contains approximately the same number of objects as that used by Miller et al. (2001), while probing a larger volume. Recently, Hütsi (2010) reported a 2σ detection of BAOs in the maxBCG galaxy cluster survey, which probes a larger effective volume than the REFLEX II sample.

Finally, regarding the redshift incompleteness of the REFLEX II catalogue mentioned in Section 2.1, we verified that our results are not substantially modified when the power spectrum is measured after randomly subtracting up to 20 per cent of the total number of clusters.

3.2 Covariance matrix

The determination of the covariance matrix of the power spectrum is a key step towards obtaining constraints on cosmological parameters. Its determination represents a non-trivial task both from theoretical and from numerical perspectives. From an analytical point of view, the covariance matrix can be decomposed into a Gaussian component, which depends on the measured power spectrum, and a non-Gaussian contribution related to the bispectrum and trispectrum (Matarrese, Verde & Heavens 1997; Verde & Heavens 2001; Smith 2008). On large scales, which are well described by linear perturbation theory, these non-Gaussian contributions vanish. On small scales, however, the non-linear evolution introduces coupling between Fourier modes generating signatures of non-Gaussianities. Hence, to precisely determine the covariance matrix, it is necessary to have a model for these high-order statistics, together with redshift distortions, survey window function effects, beat-coupling effects (Rimes & Hamilton 2006; Takayashi et al. 2009) and correlations introduced by bin averages (Meiksin & White 1999). From the numerical side, recent experiments with N-body simulations (e.g. Takayashi et al. 2009) have shown that large numbers of mock catalogues (or realizations) are required for a precise determination of the covariance matrix as needed to constrain cosmological parameters.

We used our ensemble of 100 mock catalogues to obtain an estimate of the bin-averaged covariance matrix $\hat{C}(k_i, k_j)$ of the REFLEX II power spectrum by

$$\hat{C}(k_i, k_j) = \frac{1}{N_{\rm m} - 1} \sum_{n=1}^{N_{\rm m}} \left(\hat{P}_i^n - \bar{P}_i\right)\left(\hat{P}_j^n - \bar{P}_j\right), \qquad (13)$$

where $\hat{P}_i^n = \hat{P}^n(k_i)$ is the measured power spectrum in the nth mock catalogue in the bin centred at k_i and $\bar{P}_i$ is the mean power spectrum from the ensemble of mocks at the same bin. As an example, Fig. 5 (panel a) shows the correlation coefficients r_{ij} defined from the covariance matrix via $\hat{r}_{ij} = \hat{C}_{ij}/(\hat{C}_{ii}\hat{C}_{jj})^{1/2}$ for $L_3^{\rm min}$ (upper triangular part) and $L_6^{\rm min}$ (lower triangular part). For comparison, panel (c) shows the correlation matrix inferred from the clustering of the illuminated haloes in the L-BASICC II simulation for the same luminosity cuts. The covariance matrix of the mocks contains important off-diagonal terms which arise from the mode coupling induced by the window function. All the statistical analyses performed in this work are based on the covariance matrix defined by equation (13).

FKP derived an approximated expression for the variance of the spherically averaged power spectrum under the assumption that the Fourier modes are Gaussian-distributed. This is given by

$$\frac{\sigma^2(k)}{P(k)^2} = \frac{2}{V_k V_{\rm eff}(k)}, \qquad (14)$$

where $V_k \approx 4\pi\, k^2 \delta k/(2\pi)^3$ is the volume of a spherical shell of width $\delta\, k$ and $V_{\rm eff}(k)$ is the effective (coherence) volume probed by

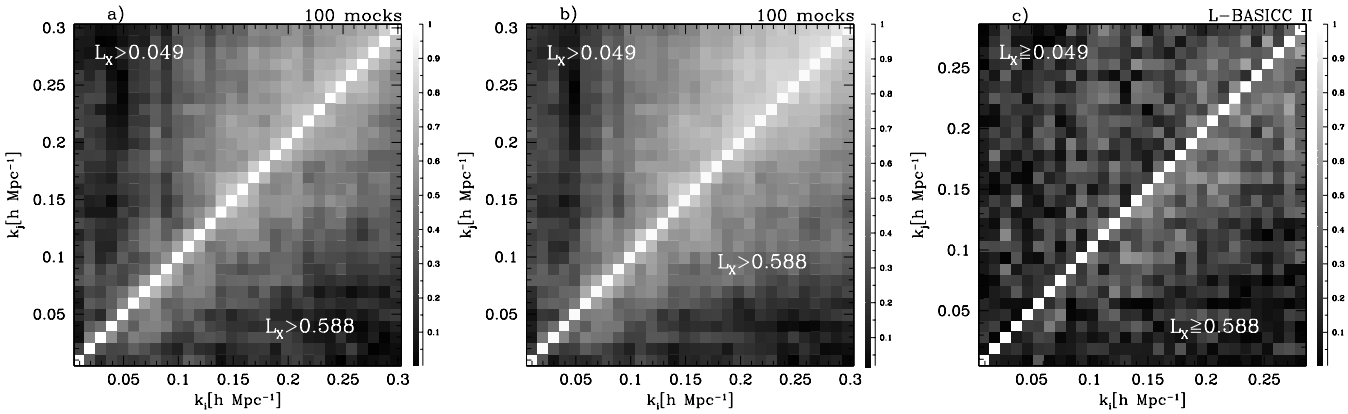

Figure 5. Comparison of the correlation matrix $|r(k_i, k_j)|$ of the power spectra measured with (panel a) the FKP estimator and (panel b) the PVP estimator (see Section 4.2) for two luminosity cuts. Panel (c): correlation matrix determined from the illuminated dark matter haloes of the L-BASICC II simulation with the same luminosity cuts.

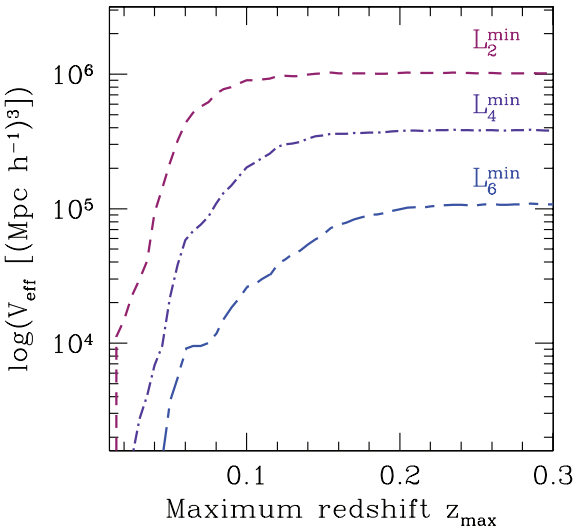

Figure 6. Effective volume probed by the REFLEX II sample (see equation 15) as a function of the maximum redshift for three different cuts in luminosity.

the survey at a scale k, defined by Tegmark (1997) as

$$V_{\rm eff}(k) = \int \left[\frac{\bar{n}(\boldsymbol{r})P(k)}{1 + P(k)\bar{n}(\boldsymbol{r})}\right]^2 {\rm d}^3 r. \qquad (15)$$

Equation (14) assumes that the power spectrum $P(k)$ is smooth on scales δk and applies for wavenumbers $k_i \gg \delta k$. Fig. 6 shows the effective volume for different luminosity cuts as a function of the maximum redshift of the sample. As pointed out in Section 2.3, the effective volume gained by including objects with redshifts $z \geq 0.22$ is very small and only leads to an increase in the shot-noise.

Fig. 7 shows a comparison of the theoretical variance computed using equation (14) with that derived from the diagonal elements of the covariance matrix of the mocks (equation 13) for the luminosity cuts defined in Section 2.2. The theoretical predictions were computed using a linear theory power spectrum with an amplitude rescaled to match that of the REFLEX II measurements for the corresponding luminosity cut. This comparison shows a very good agreement between the results obtained from the ensemble of mocks and the theoretical prediction for all values of $L^{\rm min}$. Equation (14) thus provides a good estimate of the error bars in the measured power spectra.

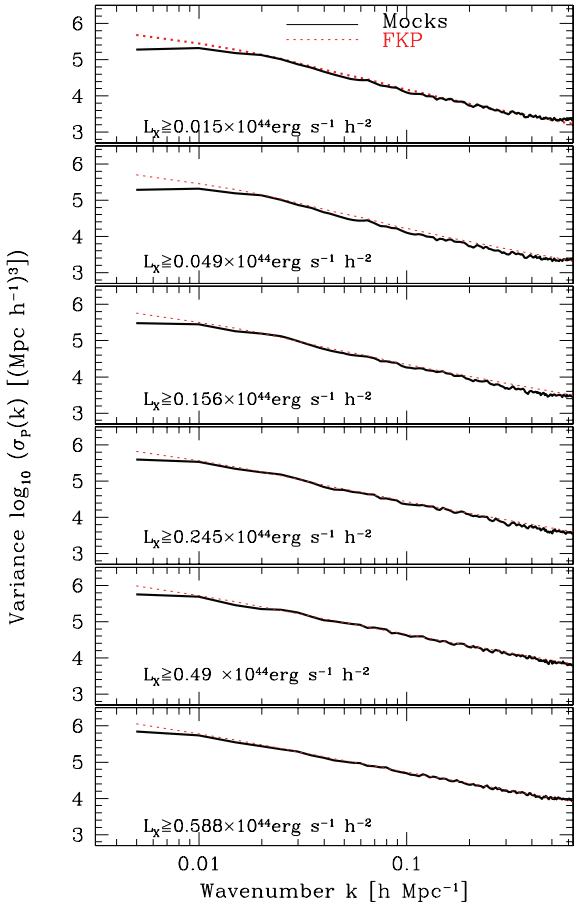

Figure 7. Bin-averaged standard deviation $\sigma_{\rm p}(k)$: solid line represents the standard deviation determined from the set of mock catalogues following equation (13). The dotted line shows the prediction from equation (14).

4 UNDERSTANDING THE REFLEX II POWER SPECTRUM

In this section, we use our ensemble of mock catalogues to understand what can be expected from a measurement of the power spectrum in the REFLEX II catalogue. Section 4.1 deals with a theoretical model for the luminosity dependence of the bias. In Section 4.2, we analyse the possible presence of a scale-dependent

systematic bias induced by the flux-limited selection. Finally, Section 4.3 describes a model for the full shape of the power spectrum, including the distortions introduced by non-linear evolution.

4.1 A theoretical prediction of luminosity bias

Assuming that on the scales of interest the underlying halo-mass bias is scale-independent, the power spectrum of galaxy clusters of a given luminosity L_X and at a given redshift z can be written as

$$P_{cl}(k, z; L_X) = b^2(L_X, z) P_{mat}(k, z), \quad (16)$$

where $P_{mat}(k, z)$ is the matter power spectrum (we now drop the redshift dependence of these factors for simplicity). The luminosity bias $b(L_X)$ is given in terms of the halo-mass function $n(M)$ and the underlying halo-mass bias $b(M)$ as (e.g. Cooray 2006):

$$b(L_X) = \frac{\int n(M) b(M) p(L_X|M)\, dM}{\int n(M) p(L_X|M)\, dM}. \quad (17)$$

Here $p(L_X|M)$ represents the conditional probability distribution of assigning an X-ray luminosity L_X to a dark matter halo of mass M. As described in Section 2.3, for our mock catalogues, $p(L_X\,|M)$ is given by a lognormal distribution with a mean given by equation (6) and a scatter including an intrinsic dispersion $\sigma_{\ln L} = 0.26$ and a 20 per cent luminosity error added in quadrature. In equation (17), the numerator is the theoretical prediction for the X-ray luminosity function

$$\Phi(L_X) = \int n(M) p(L_X|M)\, dM, \quad (18)$$

given by the halo-mass function and the mass–luminosity relation.

In order to test the predictions of equation (17), we used the 50 realizations of the L-BASICC II to measure the absolute luminosity bias. We assigned luminosities to the dark matter haloes using the calibrated mass–luminosity relation described in Section 2.3. We then measured the halo power spectrum $\hat{P}_{cl}(k; \Delta L_X)$, in real space, by splitting the sample in luminosity bins of width ΔL_X. We used the measurements of the real-space dark matter power spectrum of the same simulations to determine the ratios

$$\hat{b}(\Delta L_X) \equiv \sqrt{\frac{\hat{P}_{cl}(k, \Delta L_X)}{\hat{P}_{mat}(k)}}. \quad (19)$$

For this we used Fourier modes in the range $0.01 \leq k/(h\,\mathrm{Mpc}^{-1}) \leq 0.1$, where this ratio is compatible with a scale-independent bias factor. The obtained measurements are shown by the filled circles in Fig. 8.

The measured bias factors can be estimated by integrating equation (17) within the given luminosity bin

$$b(\Delta L_X) = \frac{\int_{\Delta L_X} \Phi(L_X) b(L_X)\, dL_X}{\int_{\Delta L_X} \Phi(L_X)\, dL_X}, \quad (20)$$

where $\Phi(L_X)$ is given by equation (18). This prediction is shown by the solid line in Fig. 8. For this we used the mass function from Jenkins et al. (2001) and the halo bias from Tinker et al. (2008), which provide an excellent description of these quantities in the L-BASICC II simulations. There is an excellent agreement between the theoretical $b(\Delta L_X)$ and the measurements obtained from the simulations. This agreement depends on the accuracy with which the M–L_X relation is known.

Under the assumptions of linear evolution and the distant observer approximation, the cluster power spectrum in redshift space is a boosted version of its real-space counterpart, $P^s_{cl}(k;\Delta L_X) = S(\Delta L_X) P_{cl}(k;\Delta\, L_X)$ (Kaiser 1987), where

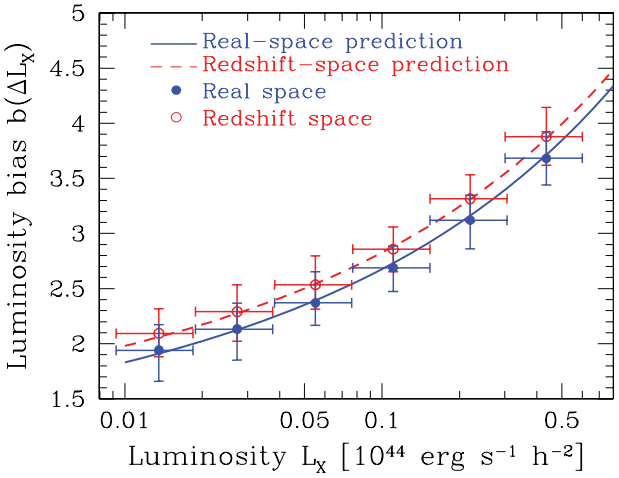

Figure 8. Measured luminosity bias $\hat{b}(\Delta L_X)$ from the L-BASICC II simulation in real space (filled points) and redshift space (open points). Solid and dashed lines represent the prediction from equations (17) and (21), respectively.

$$S(\Delta L_X) = 1 + \frac{2}{3}\frac{f}{b(\Delta L_X)} + \frac{1}{5}\left[\frac{f}{b(\Delta L_X)}\right]^2, \quad (21)$$

where $f \equiv \mathrm{d}\,\ln D(a)/\mathrm{d}\,\ln a$ is the growth index (e.g. Wang & Steinhardt 1998) and $D(a)$ is the growth factor (e.g. Peebles 1980). The open circles in Fig. 8 show the bias factors $b^s(\Delta L_X)$ estimated from the L-BASICC II simulations as in equation (19) using the redshift-space halo power spectrum $\hat{P}^s_h(k, \Delta L_X)$. The dashed line in this figure corresponds to the theoretical prediction for this quantity, given by $b(\Delta L_X)^2 S(\Delta L_X)$. The agreement between this prediction and the results from the N-body simulations shows the validity of this simple treatment of the redshift-space distortions.

The results of equations (20) and (21) can also be used to estimate the effective bias of a power-spectrum measurement in the REFLEX II catalogue for a given luminosity cut L^{min}. In order to achieve this, we first write the cluster power spectrum in redshift space at a given redshift z in terms of the linear dark matter power spectrum at $z = 0$ as

$$P^s_{cl}(k, z; > L^{min}) = b^s(> L^{min}, z)^2 P_{mat}(k, z = 0), \quad (22)$$

where

$$b^s(z, > L^{min})^2 = b(> L^{min}, z)^2 S(z, > L^{min}) D^2(z). \quad (23)$$

In this expression, we take into account that the minimum luminosity included in the sample varies with z, following the REFLEX II selection function. Accordingly, we determine the bias $b(z, > L^{min})$ following equation (20) with the red-shift dependence given by the REFLEX II sensitivity map:

$$b(z, > L^{min}) = \frac{1}{\bar{n}(z, > L^{min})} \int_{\hat{L}(z)}^{\infty} \Phi(L) b(L)\, dL\,, \quad (24)$$

where the mean number density $\bar{n}(z, > L^{min})$ and the lower integration limit $\hat{L}(z)$ are given by equations (4) and (5), respectively. Note that $\hat{L}(z)$ should depend not only on the redshift, but also on the angular position, according to the REFLEX II sensitivity map. However, in order to give an estimate of the effective bias at a fixed redshift, we made an average of the values of $L^{min}(\boldsymbol{r})$ of all the N_{pix} pixels within the REFLEX II mask. Individual pixels displayed small differences compared to the average in the final result.

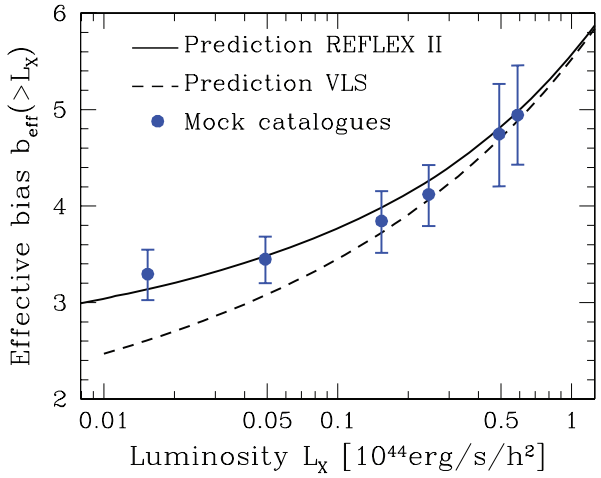

Figure 9. Effective luminosity bias measured from the REFLEX II mock catalogues (filled circles with error bars). The solid line shows the prediction from equation (25) with the fiducial values $\sigma_{\ln L} = 0.26$ and constant luminosity error of 20 per cent. The dashed line is the prediction for a VLS.

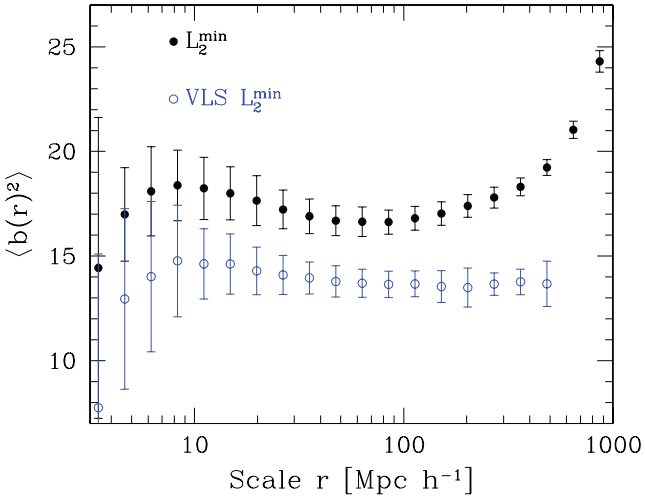

Figure 10. Mean squared luminosity bias for pairs separated by a scale r in the REFLEX II mock catalogues, for the subsample $L_2^{\rm min}$ (filled circles) and its corresponding VLS (open circles).

The effective bias of the full sample will then be given by the average of the bias factors of equation (24) over the observed volume as (e.g. Moscardini et al. 2000; Suto, Magira & Yamamoto 2000):

$$b_{\rm eff}(>L^{\rm min})^2 = \frac{\int_z [\bar{n}(z,>L^{\rm min}) b^{\rm s}(>L^{\rm min},z)]^2 \frac{{\rm d}V}{{\rm d}z}\,{\rm d}z}{\int_z \bar{n}(z,>L^{\rm min})^2 \frac{{\rm d}V}{{\rm d}z}\,{\rm d}z}, \qquad (25)$$

where the integrals are evaluated in the redshift interval of the sample with a volume element ${\rm d}V/{\rm d}z = r(z)^2/H(z)$ according to our fiducial cosmology. This therefore allows us to write a prediction for the observed power spectrum from a subsample characterized by the luminosity cut $L^{\rm min}$ as

$$P_{\rm cl}(k;>L^{\rm min}) = b_{\rm eff}(>L^{\rm min})^2 P_{\rm mat}(k,z=0). \qquad (26)$$

The solid line in Fig. 9 shows the prediction for the effective bias of the REFLEX II catalogue as a function of the minimum luminosity $L^{\rm min}$ computed using equation (25) [setting $D(z) = 1$, since, by construction, the mock catalogues assume no redshift evolution]. For comparison, the dashed line in Fig. 9 represents the equivalent prediction for a volume-limited sample. Equation (25) gives an excellent description of the direct measurements obtained from the mock catalogues (shown by the filled circles). Then, this model provides a means to extract the important cosmological information contained in the amplitude of the measured REFLEX II power spectrum.

4.2 Systematics: distortions induced in a flux-limited sample

Due to the flux-limited nature of the REFLEX II catalogue, large scales might be probed predominantly by the most-luminous clusters, with a higher clustering amplitude. This would artificially increase the measured power spectrum on large scales, introducing a scale-dependent distortion with respect to the volume-limited case. Schuecker et al. (2001) analysed this problem in detail for the REFLEX sample and concluded that no significant effect can be detected for scales $r < 150\,{\rm Mpc}\,h^{-1}$. In this section, we perform a similar analysis on the REFLEX II sample. As the REFLEX II sample spans a wider range of luminosities, and covers a larger volume than that used by Schuecker et al. (2001), it is necessary to test whether this systematic effect can affect our measurements.

Fig. 10 shows the number of pairs with separation r weighted by the individual biasing factors of the pair members (computed using equation 17) determined from the mock catalogues, yielding the average squared bias factors

$$\langle b^2(r)\rangle = \frac{1}{n(r)} \sum_{i,j} b(L_i) b(L_j), \qquad (27)$$

where the sum is done over pairs separated by scales in the range $r - \frac{1}{2}\Delta < |r_i - r_j| < r + \frac{1}{2}\Delta$ and $n(r)$ is the number of clusters in the same interval. The closed circles show the results obtained from the sample with minimum luminosity $L_2^{\rm min}$ (see Table 1), while the open circles correspond to the equivalent measurement from the VLS determined by the same minimum luminosity. The error bars are drawn from the standard deviation of the ensemble. Two prominent features can be observed from Fig. 10. On the one hand, there is an increase in the mean bias on scales $r \approx 10\,{\rm Mpc}\,h^{-1}$. This is understood as to show that pairs of clusters separated by these scales have at least one cluster with luminosity bias higher than the mean value of the sample. This is therefore a consequence of gravitational clustering. On scales smaller than $r \sim 9\,{\rm Mpc}\,h^{-1}$, the mean bias decreases as a consequence of the halo exclusion (e.g. Porciani et al. 1998). This feature is more evident in the subsample $L_2^{\rm min}$ than in its corresponding volume-limited counterpart, due basically to the low volume sampled by the latter. On the other hand, it can be clearly seen that, on scales $r \gtrsim 150\,{\rm Mpc}\,h^{-1}$, a systematic increase in the average squared bias factor exists in the flux-limited sample compared with the volume-limited case. This is a direct consequence of the flux-limited nature of the survey. Naively, the scale where this flux-selection distortion is relevant would correspond to $k = 2\pi/r = 0.04\,h\,{\rm Mpc}^{-1}$, suggesting that for wavenumbers larger than this limit, no scale-dependent distortion affects the measurements from the REFLEX II catalogue. Comparing with other subsamples, we observe that this distortion is damped in the high-luminosity cuts, which almost behave like volume-limited samples (see Fig. 2).

To analyse this issue in more detail, we used the FKP estimator as implemented by Percival, Verde & Peacock 2004 (hereinafter PVP). This is also a minimal variance weighting estimator which takes into account the absolute luminosity bias (or the relative bias to some luminosity $\bar{L}$) to obtain an estimate of the power spectrum of the underlying matter (or correspondingly, the power

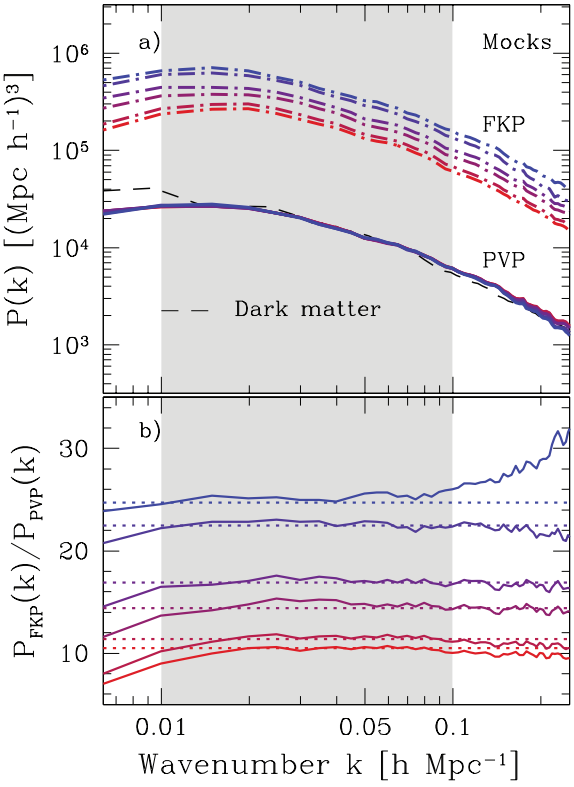

Figure 11. (a) Comparison of the resulting mean power spectrum from the mock sample using the PVP estimator (solid lines) and the FKP result (dot–dashed lines) for our six cuts in luminosity defined in Table 1. The dashed line represents the measurement of the dark matter power spectrum of the L-BASICC II simulations. The shaded region shows the scales where the absolute bias is fitted $[0.01 \leq k/(h\,\mathrm{Mpc}^{-1}) \leq 0.1]$. (b) Ratio of FKP power spectra to the PVP measurements for the six luminosity cuts.

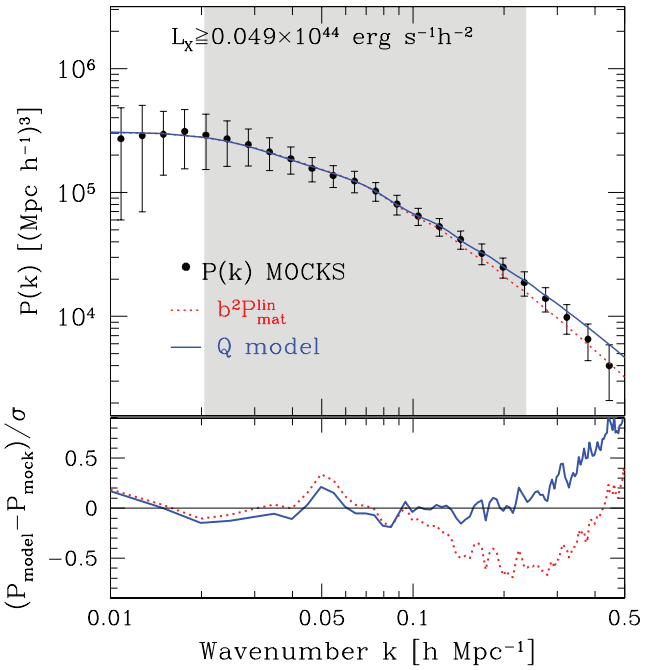

Figure 12. Q-model description of the mock power spectrum. The shaded region shows the scale where the Q-model was used to fit the mean power spectrum from the mock catalogues. The bottom panel shows the ratio of the difference between the Q-model and the measurements to the standard deviation from the mocks.

spectrum of objects with luminosity $\tilde{L}$), free of the distortions induced by the flux-limited selection of the sample. Recently, Cai, Bernstein & Sheth (2010) generalized this estimator by introducing a mass-dependent weighting scheme that minimizes the stochasticity between the cluster (or galaxy) field and the underlying matter distribution. For the goal of this section, it is enough to use the PVP estimator.

Fig. 11 (panel a) shows a comparison of the mean power spectra obtained by the FKP (dot–dashed lines) and PVP (solid lines) algorithms for the different luminosity cuts defined in Table 1 in our ensemble of mock catalogues. In the PVP method, we weighted each object by the inverse of its luminosity bias, computed using a fit to the redshift-space results shown in Fig. 8. The shaded area in Fig. 11 represents the range of scales used to measure these bias factors $[0.01 \leq k/(h\,\mathrm{Mpc}^{-1}) \leq 0.1]$. This produces a power spectrum normalized as that of the dark matter distribution (shown by the dashed line in Fig. 11). Panel (b) shows the ratios between the mean power spectra obtained using the FKP and PVP estimators for each luminosity cut. In the absence of a scale-dependent distortion, these ratios should correspond to the bias factors $b^2_{\rm eff}$ ($>L_{\rm min}$) shown by the dotted lines. These ratios show no clear signature of a scale-dependent distortion for $k \leq 0.02\,h\,\mathrm{Mpc}^{-1}$. Contrary to what might be expected from this systematic effect, Fig. 11 shows a weak indication of a decrease in power on large scales for the lower luminosity cuts, which is smaller than the standard deviation of the measurements. From this analysis, we conclude that no significant distortion is introduced in the shape of the power spectra estimated with the FKP method. Note, however, that this statement applies exclusively to the REFLEX II catalogue, as such an effect has been detected in galaxy surveys (e.g. Tegmark et al. 2006; Percival et al. 2007). Given the lack of systematic distortions in the FKP measurements, we chose to use the FKP estimator to analyse the data from the REFLEX II catalogue. Fig. 5 (panel b) shows the correlation matrix inferred from the ensemble of mock catalogues of the power spectra for two luminosity cuts obtained using the PVP estimator. A comparison with panel (a) shows that the PVP estimator induces slightly higher correlations between Fourier modes compared to the FKP case.

4.3 Modelling the shape of $P(k)$

In this section, we use our ensemble of mock catalogues to test a model of the shape of the REFLEX II power spectrum. We focus on the clusters with luminosities greater than $L_2^{\rm min}$. The filled circles in Fig. 12 show the mean redshift-space power spectrum of the mocks for this luminosity cut with error bars determined from the standard deviation of the ensemble. It can be clearly seen that this measurement exhibits an excess of power at small scales with respect to the predictions from linear perturbation theory, shown by the dashed line. This is due to the combined effect of non-linear evolution and redshift-space distortions.

In recent years, the distortions in the shape of the power spectrum produced by these effects have been intensively studied using large N-body simulations and recent advances in perturbation theory (e.g. Crocce & Scoccimarro 2006; Smith, Scoccimarro & Sheth 2007; Angulo et al. 2008; Sánchez, Baugh & Angulo 2008a; Montesano, Sánchez & Phleps 2010). These analyses have produced accurate descriptions of these distortions to the level of accuracy demanded by forthcoming surveys, which will probe volumes much larger than that of present-day catalogues. Due to the moderate

volume probed by the REFLEX II catalogue (in comparison to the volume probed by current galaxy redshift surveys), percent-level accuracies in the treatment of these effects are not required.

We now test whether the Q-model of Cole et al. (2005) (modified as in Sánchez et al. 2008a) can provide a good description of the non-linearities observed in the power spectra of our mock catalogues. In this model, the shape of the cluster power spectrum is given by

$$P_{\rm cl}(k, > L) = b_{\rm eff}(> L)^2 \left(\frac{1 + Qk^2}{1 + Ak + Bk^2} \right) P_{\rm mat}^{\rm lin}(k), \qquad (28)$$

where $P_{\rm mat}^{\rm lin}(k)$ is the linear theory matter power spectrum.

Although this model was originally developed and calibrated to describe the power spectrum of the 2dFRGS, its application has been extended to the analysis of other samples (e.g. Tegmark et al. 2006; Padmanabhan et al. 2007). In particular, Sánchez & Cole (2008) showed that this model can give a good description of the clustering of the luminous red galaxy sample from the SDSS even though it was not specifically designed to do so. At the same time, this model does not give a good description of the shape of $P(k)$ for the main galaxy sample in the SDSS. The results from the application of the Q-model to N-body simulations show that it can correctly describe the clustering of dark matter haloes above a given mass threshold (Tegmark et al. 2006).

We follow Cole et al. (2005) and fix the value of $A = 1.4$ as obtained from the analysis of N-body simulations, while Q and B are left as free parameters whose values will depend on the limiting luminosity of the sample. We assumed all the cosmological parameters to be known and fitted for Q and B, marginalizing analytically over the amplitude (as described in Lewis & Bridle 2002). From this analysis, we obtain the values $Q = 24.9 \pm 1.1$ and $B = 12.0 \pm 2.1$, corresponding to the subsample defined by $L_2^{\rm min}$. The best-fitting model obtained this way is shown by the solid line in Fig. 12. It can be clearly seen that the model of equation (28) gives an accurate description of the shape of the mean power spectrum from our ensemble of mock catalogues. This can also be seen in panel (b) of the same figure, where we show the ratio of the difference between the mean mock power spectrum and the best-fitting model to the variance from the ensemble. The parameters B and Q fitting the power spectrum of the subsample $L_2^{\rm min}$ follow a degeneracy that can be described approximately by $B(Q) = 0.805Q - 8.15$. This degeneracy is maintained if the amplitude of the model is fixed according to equation (25). We can thus use this degeneracy to reduce the number of degrees of freedom when constraining cosmological parameters using the measured power spectrum. The best-fitting value of Q increases with the limiting luminosity of the sample, varying from $Q = 20.7 \pm 0.9$ for $L_1^{\rm min}$ to $Q = 44.9 \pm 2.3$ for $L_6^{\rm min}$. The general trend in the degeneracy $B(Q)$ is maintained for different luminosity cuts. In Section 5.3, we compare the predictions of this model with the measurement of the REFLEX II power spectrum. We have explicitly tested that, by adopting a different value for A, the best-fitting value for the parameter Q, and the degeneracy between Q and B are slightly changed, while providing equally good fits to the data.

5 ANALYSIS OF THE REFLEX II POWER SPECTRUM

5.1 Measurements

The measured power spectrum for the REFLEX II sample with limiting luminosity $L_1^{\rm min}$ is shown by the filled points in Fig. 13 with error bars drawn from the FKP method (see equation 14). The solid line represents a ΛCDM linear power spectrum convolved with the window function of the survey. This theoretical prediction was computed using the fitting formulae of Eisenstein & Hu (1998), with amplitude rescaled to match that of the REFLEX II measurement. This simple exercise shows that the shape of the REFLEX II power spectrum is consistent with the predictions of the ΛCDM cosmological model.

Fig. 13 also shows a new estimation of the power spectrum of the original REFLEX sample (open triangles). The REFLEX power spectrum has a higher amplitude, as expected from the higher flux limit of this sample, and its shape is in good agreement with that of the REFLEX II measurement. The larger volume probed by the new catalogue reduces the impact of cosmic variance on large scales, where the REFLEX II power spectrum exhibits a higher amplitude than the measurement in the original REFLEX sample.

Fig. 13 also shows the galaxy power spectrum measured from the 2dFGRS (Cole et al. 2005). The dashed line represents the same ΛCDM power spectrum as described above, convolved with the 2dFGRS window function. This shows that, once their respective window functions have been taken into account, the large-scale ($k < 0.1\,h\,{\rm Mpc}^{-1}$) shapes of the REFLEX II power spectrum and that inferred from the 2dFGRS are in good agreement and can be described with the same cosmological model. At smaller scales, redshift-space distortions and non-linear evolution produce deviations in the shapes of these power spectra.

Fig. 14 shows a comparison of the measured REFLEX II power spectra (points with error bars) for the six cuts in luminosity described in Section 2.2 and the corresponding mean power spectra from the mock catalogues (solid lines), with their corresponding 1σ standard deviation (shaded regions). The error bars of the REFLEX II power spectrum correspond to the theoretical prediction of the FKP method (see section 3.2). We observe that the spectra measured in the mocks are compatible within 1σ with the REFLEX II clustering up to $k \approx 0.3\,h\,{\rm Mpc}^{-1}$ for all luminosity cuts. Note that the mocks were only calibrated to follow the X-ray luminosity function of the REFLEX II sample. This agreement allows us to use the covariance matrices inferred from the ensemble of mock catalogues when analysing the REFLEX II measurements.

On small scales, the power spectra inferred from the mock catalogues are affected by the halo exclusion effect. Dark matter haloes in the simulations have been counted as separate entities when they did not overlap with their radii of $r_{\rm FoF}$. On the other hand, in the REFLEX II catalogue, clusters have been treated as distinct if their X-ray emission does not significantly overlap. Due to the short exposures in the RASS, the outer boundary of the X-ray emission (in two dimensional images, which is significantly smaller than the aperture radius determined from one-dimensional profiles) is smaller than the radii of r_{500}. This produces differences between the REFLEX II power spectra and the results from the mock catalogues on scales $k > 0.2\,h\,{\rm Mpc}^{-1}$.

Regarding the redshift incompleteness of the REFLEX II catalogue (around 10 per cent), we verified that our results are not substantially modified when the power spectrum is measured after randomly subtracting up to 20 per cent of the total number of clusters.

5.2 Amplitude of the REFLEX II $P(k)$

Fig. 15 shows the measurements of the REFLEX II power spectra for three of the subsamples defined in Table 1. The increase in the amplitude with increasing minimum luminosity can be clearly seen, showing the signature of luminosity bias.

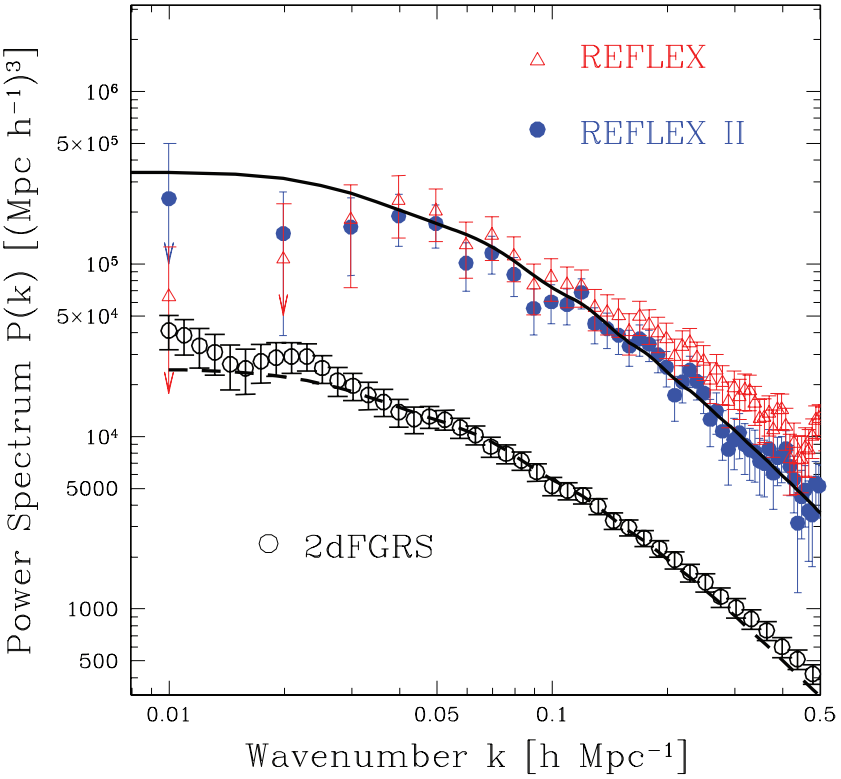

Figure 13. REFLEX II power spectrum (filled circles with error bars) for clusters with luminosities $L_X > L_1^{min}$. The REFLEX power spectrum is shown by the open triangles. The error bars for these two measurements are taken from equation (14). For comparison, we also show the measured power spectrum from the 2dFGRS taken from Cole et al. (2005) (open circles). The solid and dashed lines represent the ΛCDM power spectrum convolved with the REFLEX II and the 2dFGRS window function, respectively, and adjusted to match the corresponding spectra. Error bars exceeding the range of the plot are represented by arrows.

In Section 4.1, we showed that the measurements of the effective bias of the REFLEX II mock catalogues are well described by the predictions of equation (25). In this section, we confront this prediction with the power spectra measured from the REFLEX II sample. In order to avoid using the underlying dark matter power spectrum, we test equation (25) by means of the relative luminosity bias $r(L_X)$ defined as the ratio of the power spectrum of the subsample defined by a minimum luminosity L_X to that of clusters with luminosities greater than a reference value $\tilde{L}_X$:

$$r(L_X) \equiv \frac{b_{eff}(> L_X)}{b_{eff}(> \tilde{L}_X)}. \quad (29)$$

The results are shown in Fig. 16. The open squares show the measurements from the REFLEX II data and the filled points correspond to the respective measurement from the mock catalogues. The solid line shows the prediction from equation (25), while the dashed line is the prediction of the effective bias for a VLS. The prediction from equation (25) provides a good description of the REFLEX II measurements in the low luminosity cuts. For the last two luminosity cuts, the agreement is not as good, although the measured bias factors are consistent with the theoretical prediction within the errors. As can be seen in Fig. 14, the spectra measured from these luminosity cuts show a low amplitude at scales $k \sim 0.1\,h\,\mathrm{Mpc}^{-1}$. This dip in the power spectra, which is consistent with cosmic variance, explains why the correspondent bias measurements in Fig. 16 lie below the theoretical prediction. The agreement is improved when the bias factors are measured in the range $0.01 < k/(h\,\mathrm{Mpc}^{-1}) < 0.05$, as is shown by the open triangles in Fig. 16. These results confirm the validity of equation (25) to model the amplitude of the REFLEX II power spectrum.

Note, finally, that as the theoretical predictions for the bias are based on the mass–X-ray luminosity relation calibrated from the mock catalogues, the good agreement found with the bias factors inferred from the data suggests that for the luminosity range we have explored, the calibrated scaling relation also provides a good description of the real underlying mass–X-ray luminosity relation.

5.3 Shape of the REFLEX II $P(k)$

We used the Q-model to analyse the shape of the REFLEX II power spectrum for the subsample defined by L_2^{min}, following the same procedure as followed in Section 4.3. The best fit of the Q-model is shown by the solid line in the upper panel of Fig. 17. For this measurement, we find $Q = 24.7 \pm 1.5$ and $B = 8.6 \pm 1.1$, with a degeneracy described by $B(Q) = 0.72Q - 9.25$. This degeneracy is maintained when fixing the amplitude of the model power spectrum according to equation (25). As in Fig. 12, the bottom panel shows the ratio of the difference between the model and the measurements to the standard deviation determined from the mock catalogues. This shows that a model including a correction for non-linearities provided by equation (28) gives a better description of the shape of the REFLEX II power spectrum than the predictions from linear perturbation theory.

6 CONCLUSIONS

In this paper, we presented the measurement and analysis of the power spectrum from the new REFLEX II catalogue, which is an extension of the original REFLEX sample (Böhringer et al. 2001)

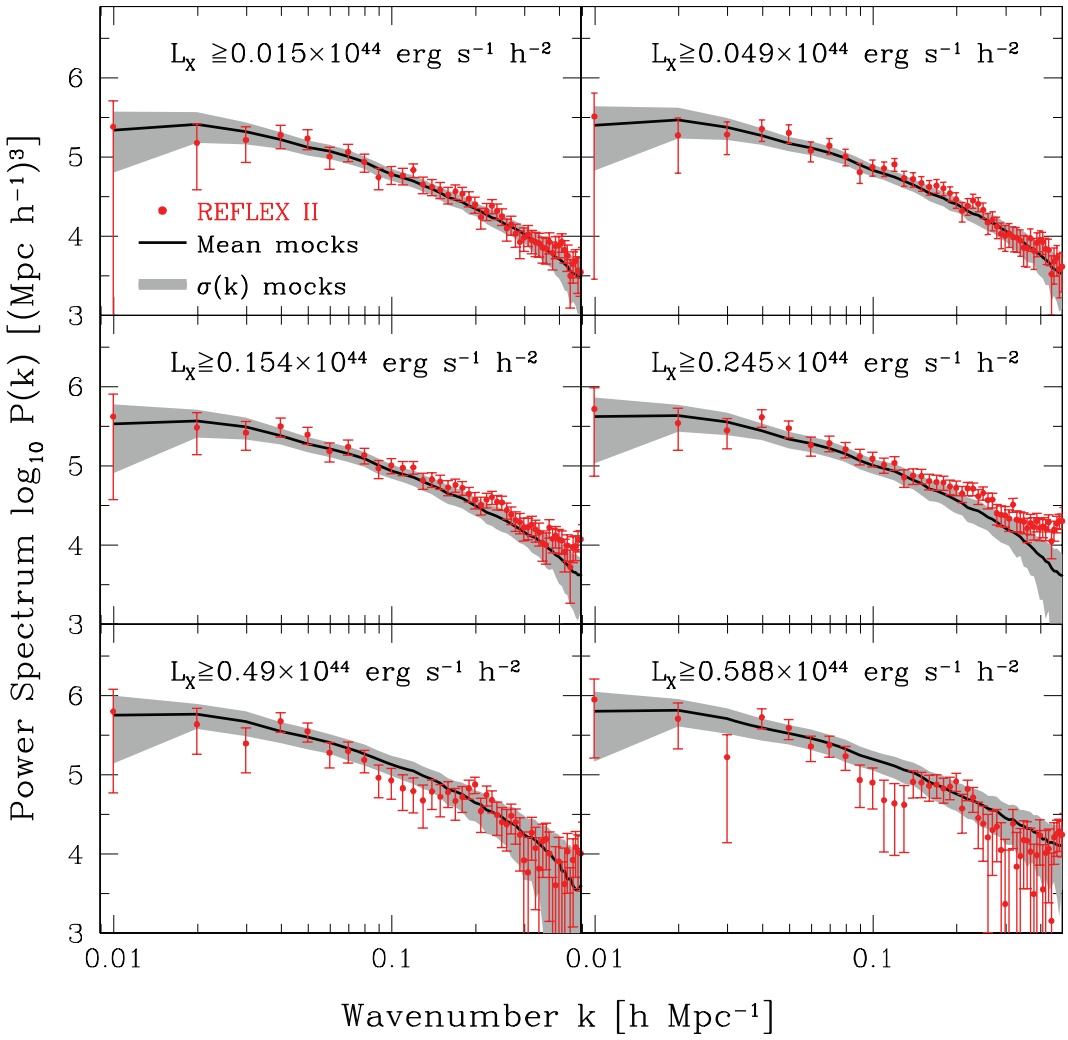

Figure 14. Measured REFLEX II power spectrum for the different subsamples defined in Table 1. The fast Fourier transform is carried out in a box of side $L_{\rm box} = 1263.8\,{\rm Mpc}\,h^{-1}$ and $P_{\rm est} = 2 \times 10^4\,({\rm Mpc}\,h^{-1})^3$. The fundamental mode is $\delta\, k = 2\pi/L_{\rm box} = 0.0049\,h\,{\rm Mpc}^{-1}$ and the Nyquist frequency is $k_{\rm Nyq} = 1.27\,h\,{\rm Mpc}^{-1}$. Points represent the REFLEX II measurements with error bars drawn from equation (14). The shaded region represents the 1σ standard deviation determined from the mocks catalogues. The solid line represents the mean mock power spectrum.

to a lower limiting flux ($1.8 \times 10^{-12}\,{\rm erg\,s^{-1}\,cm^{-2}}$). The new sample contains 911 X-ray-detected galaxy clusters of which 860 have measured redshifts in the range $0 \leq z \lesssim 0.6$ and X-ray luminosities in the range $4.9 \times 10^{40} \leq L_{\rm X}/({\rm erg\,s^{-1}}\,h^{-2}) \leq 1.96 \times 10^{45}$. The total flux and X-ray luminosities are estimated using the up-to-date scaling relations based on the REXCESS (Böhringer et al. 2007; Pratt et al. 2009).

The new sample allowed us to perform a detailed study of the full shape and amplitude of the power spectrum of X-ray-detected galaxy clusters. We complemented this analysis by using a set of 100 independent mock catalogues constructed to match the selection function of the REFLEX II survey. The clustering properties of these mock catalogues are in good agreement with those measured in the REFLEX II sample. Thus, this ensemble provides a reliable tool to test the statistical methods applied to the data. In particular, we used the mock catalogues to test a model for the luminosity dependence of bias, to construct covariance matrices of the the REFLEX II power spectrum and to analyse the possible systematic effects that might affect this measurement.

Due to the flux-limited selection of the REFLEX II survey, the clustering pattern of galaxy clusters might be affected by scale-dependent distortion, as has been observed in galaxy surveys (e.g. Tegmark et al. 2006; Percival et al. 2007). Using the mock catalogues, we have shown that these distortions might affect the clustering in configuration space (i.e. when measured with the cluster correlation function) on scales $r \geq 150\,{\rm Mpc}\,h^{-1}$, which would naively correspond to scales $k \leq 0.04\,h\,{\rm Mpc}^{-1}$ in Fourier space. In order to test the impact of this flux-selection effect on the final measurements of power spectra, we implemented the luminosity-dependent estimator of PVP, which is designed to correct for this distortion. We observed that the shape of the power spectrum measured by means of the FKP estimator does not show significant distortions compared to the results from the PVP estimator. This implies that the flux selection of the REFLEX II sample does not introduce a significant systematic effect in the measurement of the power spectrum of this catalogue.

The shape of the mean power spectrum from our ensemble of mock catalogues is in good agreement with the measured power spectrum from the REFLEX II sample and is statistically distinguishable from the linear perturbation theory predictions on intermediate scales. This implies a clear signature of non-linear evolution in the X-ray cluster spatial distribution. Nevertheless,

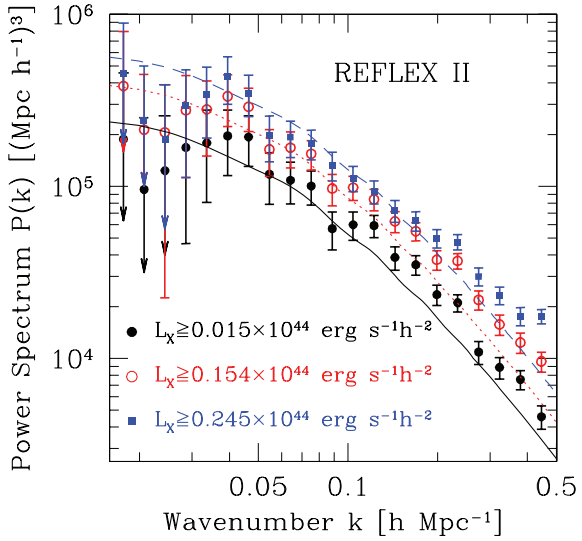

Figure 15. REFLEX II power spectrum for three different minimum luminosities. Lines represent a linear perturbation theory power spectrum with our fiducial cosmology and amplitude given by equation (25). Error bars correspond to the standard deviation drawn from the mock catalogues. Arrows denote the error bars exceeding the range of the plot.

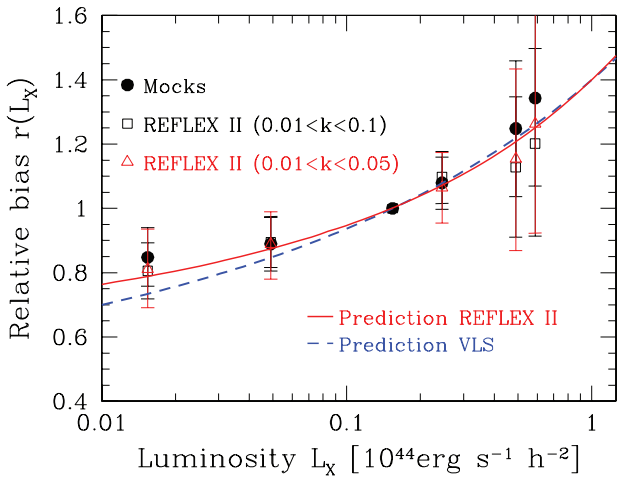

Figure 16. Relative luminosity bias measured from the REFLEX II data in the range $0.01 < k/(h\,\mathrm{Mpc}^{-1}) < 0.1$ (open squares) and $0.01 < k(h\,/\mathrm{Mpc}^{-1}) < 0.05$ (open triangles), and the mock catalogues (filled points). The reference luminosity is $\tilde{L} = L_3^{\mathrm{min}}$. The dashed line is the prediction from equation (29) for a VLS, while the solid line is the prediction from equation (25) used in equation (29).

given the level of accuracy of the measurements of power spectrum in the REFLEX II sample, it is sufficient to model these distortions using the Q-model of Cole et al. (2005). We find that this prescription provides a good description of the measurements from the mock catalogues on intermediate scales [$0.02 \leq k/(h\,\mathrm{Mpc}^{-1}) \leq 0.25$]. This model can also be used to describe the shape of the measured REFLEX II power spectrum, providing a valuable tool to extract the cosmological information contained in the shape of this statistic. The next generation of X-ray galaxy cluster surveys, such as *eROSITA*[4] and *WFXT*[5], will provide measurements of the

[4]http://www.mpe.mpg.de/heg/www/Projects/EROSITA/main.html
[5]http://wfxt.pha.jhu.edu/

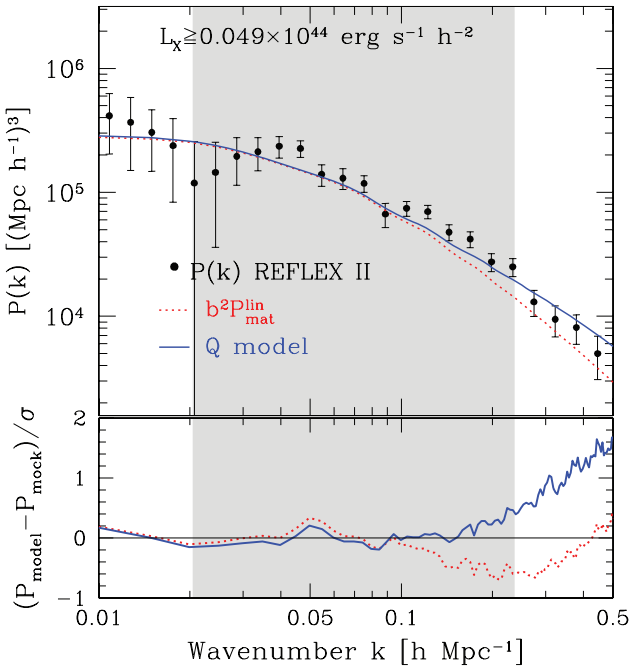

Figure 17. Best-fitting Q-model for the REFLEX II mock power spectrum (points with error bars). See Fig. 12 for description.

two-point statistics of the cluster population with higher accuracy than present-day samples, for which a more detailed modelling of non-linearities will be required (e.g. Crocce & Scoccimarro 2006; Montesano et al. 2010).

Our measurements of the REFLEX II power spectrum are compatible with the prediction of the ΛCDM cosmological model and show good agreement with the previous results from the REFLEX sample (Schuecker et al. 2001), saving the expected differences due to the lower limiting flux of the REFLEX II sample. We showed that our measurements cannot provide a statistically significant detection of BAOs, which is mainly due to the moderate volume probed by the survey (compared to the volume probed by current galaxy redshift surveys). We found that the power spectra measured from the REFLEX II sample and the mock catalogues are compatible with a scale-independent effective bias in the range of wavenumbers $0.01 \leq k/(h\,\mathrm{Mpc}^{-1}) \leq 0.1$, and that a simple theoretical prediction, based on the halo-mass bias, the halo-mass function and the mass–luminosity relation, is able to describe these measurements. This, together with the modelling of the shape of the power spectrum given by the Q-model, provides a link to the cosmological models and allows our measurements to reach their full constraining power.

ACKNOWLEDGMENTS

We thank Raúl Angulo and Carlton Baugh for providing us with the L-BASICC II simulations. AB-A acknowledges the PhD fellowship of the International Max Planck Research School in the OPINAS group at MPE. This research was supported by the DFG Cluster of Excellence 'Origin and Structure of the Universe'. This paper contains observational data obtained at the ESO La Silla observatory. We wish to thank the ESO Team for their support.

REFERENCES

Angulo R., Baugh C. M., Frenk C. S., Lacey G. C., 2008, MNRAS, 383, 755
Arnaud K. A., 1996, in Jacoby G., Barnes J., eds, ASP Conf. Ser. Vol. 101, Astronomical Data Analysis Software and Systems V. Astron. Soc. Pac., San Francisco, p. 17
Arnaud M., Pointecouteau E., Pratt G., 2005, A&A, 441, 893
Arnaud M., Pratt G. W., Piffaretti R., Böhringer H., Croston J. H., Pointecouteau E., 2010, A&A, 517, A92
Bardeen J. M., Bond J. R., Kaiser N., Szalay A. S., 1986, ApJ, 304, 15
Böhringer H. et al., 2000, ApJS, 129, 435
Böhringer H. et al., 2001, A&A, 369, 826
Böhringer H. et al., 2002, ApJ, 566, 93
Böhringer H. et al., 2007, A&A, 469, 363
Cai Y., Bernstein G., Sheth R. K., 2010, preprint (astro-ph/1007.3500)
Cavaliere A., Fusco-Femiano R., 1976, A&A, 49, 137
Cole S. et al., 2005, MNRAS, 362, 505
Collins C. et al., 2000, MNRAS, 319, 939
Cooray A., 2006, MNRAS, 365, 842
Crocce M., Scoccimarro R., 2006, Phys. Rev. D, 73, 063519
Dickey J. M., Lockman F. J., 1993, ARA&A, 28, 215
Eisenstein D., Hu W., 1998, ApJ, 496, 605
Eisenstein D. et al., 2005, ApJ, 633, 560
Feldman H., Kaiser N., Peacock J. A., 1994, ApJ, 426, 23 (FKP)
Frigo M., Johnson S., 2005, Proc. IEEE, 93, 216
Gaztañaga E., Cabré A., Hui L., 2008, MNRAS, 399, 1663
Giodini S. et al., 2009, ApJ, 703, 982
Guzzo L. et al., 2009, A&A, 499, 357
Hockney R. W., Eastwood J. W., 1988, Computer Simulation Using Particles. Adam Hilger, Bristol
Hütsi G., 2010, MNRAS, 401, 2477
Jenkins A., Frenk C., White S. D. M., Colberg J. M., Evrard A. E., Couchman H. M. P., Yoshida N., 2001, MNRAS, 312, 372
Kaiser N., 1987, MNRAS, 227, 1, 21
Kerscher M. et al., 2001, A&A, 377, 1
Komatsu E. et al., 2010, preprint (astro-ph/1001.4538)
Lewis A., Bridle S., 2002, Phys. Rev. D, 66, 103511
Lukic Z., Reed D., Habib S., Heitman K., 2010, ApJ, 692, 217
Makino N., Sasaki S., Suto Y., 1998, ApJ, 497, 555
Mantz A., Allen S., Ebeling H., Rapetti D., Drlica-Wagner A., 2010, MNRAS, 406, 1773
Matarrese S., Verde L., Heavens A., 1997, MNRAS, 290, 651
Meiksin A., White M., 1999, MNRAS, 308, 1179
Miller C., Nichol R., Batuski D., 2001, ApJ, 555, 68
Montesano F., Sánchez A. G., Phleps S., 2010, MNRAS, 408, 2397
Moscardini L., Matarrese S., Lucchini F., Rosati P., 2000, MNRAS, 316, 283
Padmanabhan N. et al., 2007, MNRAS, 378, 852
Peebles P. J. E., 1980, The Large-Scale Structure of the Universe. Princeton Univ. Press, Princeton, NJ
Percival W. J. et al., 2002, MNRAS, 337, 1068
Percival W. J., Verde L., Peacock J. A., 2004, MNRAS, 347, 645 (PVP)
Percival W. J. et al., 2007, ApJ, 657, 645
Percival W. J. et al., 2010, MNRAS, 401, 2148
Perlmutter S. et al., 1999, ApJ, 517, 565
Porciani C., Matarrese S., Luccini F., Catelan P., 1998, MNRAS, 298, 1097
Pratt G., Croston H. J., Arnaud M., Böhringer H., 2009, A&A, 498, 361
Press H., Teukolski S., Vetterling W., Flannery B., 2002, Numerical Recipes in C. Cambridge Univ. Press, Cambridge
Puchwein E., Sijacki D., Springel V., 2008, ApJ, 687, L53
Reid B. et al., 2010, MNRAS, 404, 60
Reiprich T., Böhringer H., 1999, AN, 320, 296
Riess A. G., Strolger L. G., Tony J., 2004, ApJ, 116, 665
Rimes C., Hamilton A. J. S., 2006, MNRAS, 37, 1205
Sánchez A. G., Cole S., 2008, MNRAS, 385, 830
Sánchez A. G., Lambas D. G., Böhringer H., Schuecker P., 2005, MNRAS, 362, 1225
Sánchez A. G., Baugh C. H., Percival W. J., Peacock J. A., Padilla N. D., Cole S., Frenk C. S., Norberg P., 2006, MNRAS, 366, 189
Sánchez A. G., Baugh C. M., Angulo R., 2008, MNRAS, 390, 1470
Sánchez A. G., Crocce M., Cabré A., Baugh C. M., Gaztañaga E., 2009, MNRAS, 400, 1643
Schuecker P. et al., 2001, A&A, 368, 86
Schuecker P., Böhringer H., Collins C., Guzzo L., 2003, A&A, 398, 867
Smith R., 2008, MNRAS, 400, 851
Smith R. et al., 2003, MNRAS, 341, 1311
Smith R., Scoccimarro R., Sheth R. K., 2007, Phys. Rev. D, 75, 063212
Spergel D. N. et al., 2007, ApJS, 170, 377
Stanek R., Evrard A. E., Böhringer H., Schuecker P., Nord B., 2006, ApJ, 209, 17
Stanek R., Rasia E., Evrard A. E., Pierce F., Gazzola L., 2010, ApJ, 715, 1508
Suto Y., Magira H., Yamamoto K., 2000, PASJ, 52, 249
Takahashi R. et al., 2009, ApJ, 700, 497
Tegmark M., 1997, Phys. Rev. Lett., 79, 3806
Tegmark M. et al., 2006, Phys. Rev. D, 74, 123507
Tinker J., Kravtsov A., Klypin A., Abazajian K., Warren M., Yepes G., Gottlöber S., Holz D., 2008, ApJ, 688, 709
Truemper J., 1993, Sci, 260, 1769
Tsallis C., 2009, Introduction to Nonextensive Statistical Mechanics. Springer-Verlag, New York
Verde L., Heavens A., 2001, ApJ, 553, 14
Wang L., Steinhardt P. J., 1998, ApJ, 508, 483
Warren M., Abazajian K., Holz D., Teodoro L., 2006, ApJ, 646, 881

This paper has been typeset from a TEX/LATEX file prepared by the author.